


# Evaluation and optimization of parameters in the measurement for airborne scanner using response surface method

Measurement and Control  
2019, Vol. 52(5-6) 354–368  
© The Author(s) 2019  
Article reuse guidelines:  
sagepub.com/journals-permissions  
DOI: 10.1177/0020294019837992  
journals.sagepub.com/home/mac  


Ding-bang Zhang<sup>1</sup>, Yi Zhang<sup>2,5</sup> , Zheng Shen<sup>3</sup>,  
Tao Cheng<sup>1</sup> and Yongtao Bai<sup>4</sup>

## Abstract

This paper aims to evaluate the working parameters and try to make an optimized use of the parameters which affect the measurement accuracy of airborne scanner. First, based on response surface method, three levels of configuration values of each parameter are selected, respectively, and 53 response surface experiments are designed. Second, three-dimensional coordinate errors of the scan points in each response surface experiment are calculated by comparing the coordinates measured by airborne scanner and common measuring apparatus. Third, by analyzing the experimental error through response surface method, the optimum configuration values of the parameters are determined. Meanwhile, the configuration characteristics and change laws of each parameter on three-dimensional coordinate errors are also realized. Results show that the most influencing parameters are flight height, flight speed, ground feature, aspect angle, scan frequency, and course angle. The optimum values for these parameters are found to be 46.14 m/s for flight speed, type 2 for ground feature, 88 Hz for scan frequency, 54.4° for course angle, 24.12° for aspect angle, and 215.92 m for flight height. The verification experiments showed that the predicted values from the response surface method are quite close to the experimental values, which validate the proposed approach.

## Keywords

Airborne scanner, response surface, engineering uncertainty, engineering measurement

Date received: 21 December 2018; accepted: 4 February 2019

## Introduction

Airborne scanning technology is a new remote sensing technology developed in recent years. It can quickly acquire digital surface models (DSMs) and digital ground models with high precision and spatial resolution.<sup>1,2</sup> There is an increasing number of applications of airborne scanner in, for example, geodesy, engineering surveying, urban modeling, and disaster assessment.<sup>3–6</sup> However, it is realized that the airborne scanning technology cannot be well applied unless the three-dimensional (3D) coordinate errors are well handled. The 3D coordinate errors affecting the measurement accuracy of airborne scanner mainly come from the following three uncertainty sources: (1) the differences of sensitivity of various measurement sensors contained in airborne scanner system;<sup>7–9</sup> (2) the system integration error, such as timing error of timing system,<sup>10–12</sup> or interpolation error due to different

scanning rates;<sup>13,14</sup> and (3) calculation error, such as truncation error and rounding error.<sup>15,16</sup>

Usually, if the hardware of the airborne scanner system is known, these three kinds of measurement errors can be determined in the scanning process. However, in the process of scanning, which also needs computer

<sup>1</sup>School of Civil Engineering, Hubei Polytechnic University, Huangshi, China

<sup>2</sup>Geodätisches Institut, Leibniz Universität Hannover, Hannover, Germany

<sup>3</sup>2nd Engineering Co., Ltd, Chinese Railway 11th Bureau Group, Shiyao, China

<sup>4</sup>College of Civil Engineering, Chongqing University, Chongqing, China

<sup>5</sup>Department of Civil Engineering, Tsinghua University, China

## Corresponding author:

Yi Zhang, Geodätisches Institut, Leibniz Universität Hannover, Hannover, Germany.

Email: zhang\_yi87@163.com



Creative Commons CC BY: This article is distributed under the terms of the Creative Commons Attribution 4.0 License

(<http://www.creativecommons.org/licenses/by/4.0/>) which permits any use, reproduction and distribution of the work without

further permission provided the original work is attributed as specified on the SAGE and Open Access pages (<https://us.sagepub.com/en-us/nam/open-access-at-sage>).

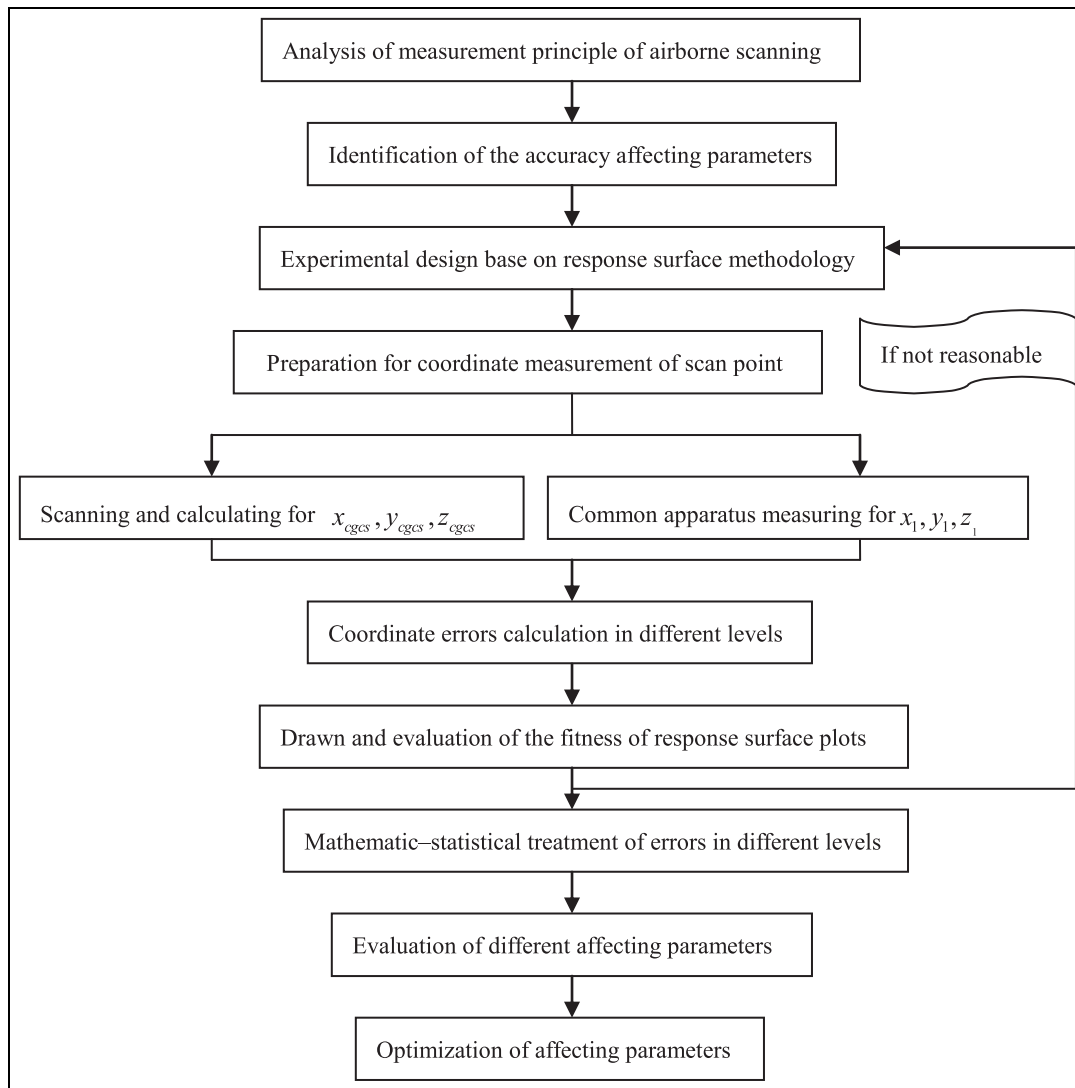


**Figure 1.** Research procedures.

calculations for the 3D coordinates, there are still more working parameters that need to be evaluated. This includes the flying height of the aircraft, the flying speed, the latitude and longitude of the aircraft, the scanning frequency of the scanner, the aspect angle of the aircraft, the course angle of scan point, and the ground feature (terrain fluctuations), which will indirectly affect the measurement accuracy of airborne scanner. Therefore, it is of great practical significance to reasonably design the setting values of various working parameters to make the measurement accuracy of the airborne scanner the best.

For analyzing the influences of these working parameters on measurement accuracy, cross-combination design and experiment studies are required. The response surface method (RSM) is one of the methods for comprehensive experimental design and mathematical modeling.<sup>17–20</sup> Multivariate analysis methods can be found in Zhang et al.<sup>21–23</sup> It could effectively reduce the number of experiments and characterizes the interaction between different working parameters. However, it has not yet applied in the airborne scanning

technology. And its efficiency of identifying the most optimum values of working parameters for the measurement is still unknown. Thus, the significance of this work is justified.

In this paper, we aim to obtain the optimal configuration values of the working parameters, the configuration characteristics, and change laws of each parameter on 3D coordinate errors for the airborne scanning system by using RSM. This work intends to provide a guidance for engineers to understand and know how to improve the measurement accuracy of airborne scanner. The detailed research steps of this research are shown in Figure 1.

## Literature review

In this section, the existing research works in the literature related to airborne scanning errors are reviewed. The literature review includes three parts. The first part summarizes the literature about the working parameters affecting the measurement accuracy of airborne

scanner. The second part discusses the use of RSM. The third part concludes the limitations of the past contributions.

### Measurement accuracy of airborne scanner

In the past, a lot of research works have done on the analysis of the influence of various measurement errors on the accuracy of airborne scanner measurement. For example, such works include the influence of laser ranging error,<sup>24,25</sup> the influence of attitude angle on measurement error of airborne platform,<sup>26–28</sup> ability of high-density laser scanning,<sup>29,30</sup> and random measurement errors on airborne laser scanning (ALS) accuracy.<sup>31,32</sup> Among these, Yang et al.<sup>19</sup> constructed a DSM by the global positioning system (GPS) and inertial measurement unit (IMU) integrated system, and evaluated the elevation accuracy of an ALS system. The conclusion showed the random attitude measurement accuracy of GPS, or IMU integrated system should be higher than 0.01 degrees (1 sigma) at least. Wu et al.<sup>33</sup> proposed a general realization method of laser ranging for micro-UAVs (unmanned aerial vehicles) and conducted the ranging experiments on measurement accuracy. The results showed the laser ranging error could be controlled and the measurement accuracy can be greatly improved with the proposed general realization method.

In addition, some literatures have studied the influence of the operating parameters on the accuracy of airborne scanner measurement. For example, in order to assess the influence of airborne scanning sensor and flight configurations on the ability to estimate the heights of trees, Næsset<sup>34</sup> utilized three different terrain models to test the effects of different preprocessing parameters on the ability to detect small trees. It was found that the standard deviation for the differences between laser-derived and field-measured tree heights was 0.16 to 0.57 m. It concluded that there are significant influences of parameters on the measurement accuracy when using airborne lasers for tree growth monitoring. Goodwin et al.<sup>35</sup> investigated the effect of a number of extrinsic parameters on the measurement accuracy of airborne scanner, including platform altitudes ranging, scan angles ranging, and footprint sizes ranging. It concluded that the accuracy and coverage of scanner observations were highly dependent on both the extrinsic parameters of the airborne scanner and the underlying structure of survey ground. Watt et al.<sup>36</sup> analyzed the precision of regressions between scanner metrics and stand metrics (mean top height,  $H_z$ ; volume,  $V$ ; and mean diameter,  $D$ ) under a range of pulse densities using digital terrain models representing two common scenarios. Wang et al.<sup>37</sup> studied the influence of attitude angle variation of airborne platform on the 3D imaging accuracy of airborne scanner. It concluded that attitude deviations had significant impact on the

accuracy of reconstructed DSM and should be suppressed or compensated in real time with effective measurements.

### RSM

RSM is a test design method proposed by Box and collaborators in chemical investigations in the 1950s.<sup>38,39</sup> It is also an efficient method for experimental design and mathematical modeling. It can be used to achieve optimal design for the input parameters by conducting tests in some representative points and build the relationship function between input parameters and the output.<sup>40</sup>

Comparing RSM with the widely used orthogonal experimental design method,<sup>41</sup> the orthogonal experiment cannot obtain the explicit function between the experimental input and output in the specified experiments.<sup>42</sup> Thus, the optimal combination of experimental factors and the optimal experimental output cannot be obtained. Moreover, when the test factors have more levels, the number of experiments needed in orthogonal design method is much more than that in RSM. The RSM has the advantages of few trials, short test period, high precision, high accuracy of regression equations, good prediction performance, and the ability to study the interaction between several factors. RSM is initially used in chemical experiments.<sup>43,44</sup> In recent years, it becomes an optimization theory method and widely applied in chemical engineering,<sup>45,46</sup> agricultural engineering,<sup>18</sup> civil engineering,<sup>47,48</sup> food engineering,<sup>45,49</sup> and other experiment sciences.<sup>17,50</sup>

### Limitation of the past contributions

From the literatures on the measurement accuracy of airborne scanner, several limitations can be spotted. The coordinate system used in airborne scanning is the Wide-Band Satellite 1984 (WGS-84) and the received signals are from Global Position System. Unfortunately, the research on the use of Chinese Geodetic Coordinate System 2000 (CGCS-2000) and Beidou Navigation Satellite System in airborne scanning is quite rare. Moreover, most literatures on the measurement accuracy of airborne scanner are focusing on the sensitivity of various measurement sensors, system integration effect, and calculations, but the working parameters (i.e. flying height of the aircraft, speed, scanning frequency, aspect angle, course angle, and ground feature) which may also significantly affect the measurement accuracy are not studied in detail in previous works.

From the literature review of RSM, it is found that RSM has never been used in the researches on the influence of working parameters on measurement accuracy of airborne scanner. The experiments using RSM in previous researches are aiming to find the optimal values of each factor and its corresponding optimal

responses. The optimal responses are always the maximum value of experiments. However, the target of the current work in this paper is to find the minimum value of coordinate error corresponding to the working parameters. The use of RSM on this topic has never been reported.

From the literature, it was found that there is no detailed report in the research about the evaluation and optimization of parameters affecting the measurement accuracy of airborne scanner. It is demanded to have a systematic research on analyzing the influence of the working parameters on the measurement accuracy in airborne scanning process and how to make optimizations in the parameter setting by using the RSM.

## Theoretical analysis

### Measurement principle of airborne scanning

Measuring devices including scanner, inertial measurement devices, and Beidou navigation satellite system are fixed on the mounting platform of the aircraft. Figure 2 illustrates the airborne scanner using the line scanning method, in which the  $O - X_S, Y_S, Z_S$  is the reference coordinate system of scanner. It can be seen from Figure 2 that the scanner emits the scanning beam to the ground, then the scan point  $P$  on the ground reflects the scanning beam back to the scan mirror. The time length of the scanning beam returning from the emitter to the receiver via the ground scan point can be collected through the timing function in scanner.<sup>51</sup> Thus, the distance  $S$  from the optical center point  $O$  of the scanner to the ground scan point  $P$  can be calculated and the associated measurement angle  $\theta$  can be measured by a photoelectric encoder in the scanner.

Based on the distance  $S$  and the associated angle  $\theta$ , the relative 3D coordinates of the ground scan point  $P$  in the reference coordinate system  $O - X_S, Y_S, Z_S$  can be calculated. In addition, the instantaneous spatial position and attitude angle of the aircraft platform are measured by emitting and receiving the signals from Beidou navigation satellite system.

Through coordinate transformation, the absolute 3D coordinates of the scan point in the CGCS-2000 can be calculated as<sup>52,53</sup>

$$\begin{bmatrix} x_{cgcs} \\ y_{cgcs} \\ z_{cgcs} \end{bmatrix} = K_{bl} \left\{ K_N \left[ K_\theta K_\delta \begin{pmatrix} 0 \\ 0 \\ S \end{pmatrix} - \begin{pmatrix} \Delta x'_b \\ \Delta y'_b \\ \Delta z'_b \end{pmatrix} \right] \right\} + \begin{bmatrix} x_b \\ y_b \\ z_b \end{bmatrix} \quad (1)$$

where  $S$  is the distance from the optical center point  $O$  to the ground scan point  $P$ ;  $x_b, y_b, z_b$  are the 3D coordinates of the beam receiving antenna at scanner in CGCS-2000;  $\Delta x'_b, \Delta y'_b, \Delta z'_b$  are the eccentric

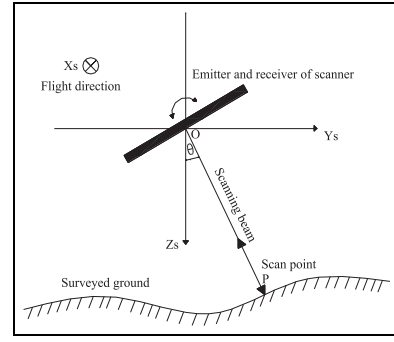


Figure 2. Illustration of airborne scanner.

displacement vectors between receiving antenna and optical center point  $O$  of the scanner;  $K_\delta$  is the rotation matrix for converting the 3D coordinates of scan point in the reference coordinate system to the inertial coordinate system;  $\delta_x, \delta_y, \delta_z$  are the rotation angles between the reference coordinate system and the inertial coordinate system;  $K_\theta$  is the rotation matrix related to the angle  $\theta$ ;  $K_N$  is the matrix for converting the 3D coordinates of scan point in the inertial coordinate system to the local coordinate system; and  $K_N = K_y(\xi)K_x(\eta)$ , in which  $\xi, \eta$  are the deviation of plumb line in vertical and horizontal directions, respectively.<sup>54</sup>  $K_{bl}$  is the matrix for converting the 3D coordinates of scan point in the local coordinate system to the CGCS-2000 system, in which  $b, l$  are the longitude and latitude of scan point, and the longitude and latitude can be converted by 3D coordinates  $(x_b, y_b, z_b)$  which are measured in Beidou navigation satellite system.

After a scanning beam is emitted from the scanner, the instantaneous data of each parameter (i.e.  $S, x_b, y_b, z_b, \theta, \delta_x, \delta_y, \delta_z, \omega, \varphi, \kappa, \xi, \eta, \Delta x'_b, \Delta y'_b, \Delta z'_b$ ) are collected by corresponding sensors. Based on equation (1), the 3D coordinates of scan point in Beidou navigation satellite system can be calculated.

### Measuring error of scan point

Certain scan points are initially identified on the scan ground by using both airborne scanner and common measuring apparatus (i.e. electronic total station is used to measure  $x, y$  coordinates, and level instrument is used to measure  $z$  coordinate). As both the measurement accuracy of electronic total station in  $x, y$  coordinates and level instrument in  $z$  coordinate is within 1 mm,<sup>54-57</sup> the value differences of  $x, y$  coordinates between airborne scanning and electronic total station measuring are deemed as the measuring errors  $(\Delta x, \Delta y)$ . The value difference of  $z$  coordinate between airborne scanning and level instrument measuring is deemed as the measuring error  $\Delta z$ . Therefore, the measuring errors of 3D coordinates can be written as

$$\begin{aligned} \Delta x &= x_{cgcs} - x_1, \Delta y = y_{cgcs} - y_1, \Delta z = z_{cgcs} - z_1, \\ \prod &= \sqrt{\Delta x^2 + \Delta y^2 + \Delta z^2} \end{aligned} \quad (2)$$

where  $\Delta x$ ,  $\Delta y$ , and  $\Delta z$  are the coordinate errors in  $x$ -,  $y$ -, and  $z$ -axes directions, respectively, and  $x_{cgcs}$ ,  $y_{cgcs}$ , and  $z_{cgcs}$  are the  $x$ ,  $y$ , and  $z$  coordinates of scan point measured by airborne scanner.  $x_1$ ,  $y_1$ , and  $z_1$  are the  $x$ ,  $y$ , and  $z$  coordinates of point measured by electronic total station and level instrument.  $\Pi$  indicates the calculated total 3D coordinate errors. All the coordinates in equation (2) are based on the definitions given in CGCS-2000.

According to equation (1) and the measurement principle of airborne scanner, flying height of aircraft, flying speed of aircraft, scanning frequency of scanner, aspect angle between scanner and scan point, course angle of aircraft, and ground condition can be listed as the working parameters affecting the measurement accuracy. Although the latitude and longitude coordinates of measured area are also influencing factors, they are difficult to be investigated as infinite experiments are required. Thus, they are not considered in the analysis.

The following will be focusing on how to obtain the optimal configuration values of the working parameters. The configuration characteristics and change laws of each parameter on 3D coordinate errors will also be investigated.

## Experiment preparation and design

### Research procedures of performing RSM

The procedures of applying the RSM as an optimization technique are given as follows: (1) identifying the independent variables affecting the measurement system and determining the lower, middle, and upper levels of the design variables; (2) carrying out the experiments according to the selected experimental matrix; (3) analyzing the experimental data by using the fit of a polynomial function; (4) evaluating the model accuracy; (5) verification of the necessity and possibility of performing a displacement in direction to the optimal region; and (6) obtaining the optimum values for each studied variable.

### Research instrument, software, and location

The research instruments include airborne scanner, electronic total station, and level instrument. The airborne scanner system used in experiments contains unmanned aircraft (P540H) and airborne scan system (AS100) which are made by Shanghai Huace Navigation Technology Ltd. The electronic total station and level instrument are Nova TS50 and LS15 made by Leica Geosystems Ltd.

The software used in this paper for the experimental design and analysis is Design-Expert 7.0. The software can be used to intuitively draw contour map and 3D graph and determine the optimization scheme of the experiments. The measured area is located in an open

area in the zone of Shiyan City, Hubei Province, China, which locates at 32°39' N and 110°47' E.

### Experimental design based on RSM

The entire experiment is divided into two parts, namely, preliminary experiments and main experiments. The aim of preliminary experiments is to determine appropriate lower, middle, and upper levels for the design variables, and analyze the influence of single design variable parameters on measurement accuracy of airborne scanner. There are six groups of preliminary experiments. In each group, the investigated parameter is a variable and others are set as recommended initial settings. The levels of speed range from 20 to 100 m/s. Period of sinusoidal wave topography (ground feature) ranges from 50 to 100 m. Scan frequency ranges from 20 to 100 Hz. Course angle ranges from 0° to 90°. Aspect angle ranges from 10° to 30° and height ranges from 100 to 500 m.

In the main experiments, a six-factor and a three-level response surface design consisting of 53 experimental runs is employed at the center point. The response surface design is following a Box–Behnken design. The effects of unexplained variability in the observed response due to extraneous factors were minimized by randomizing the order of experiments. The independent design parameters are the speed ( $N_1$ , m/s), ground feature ( $N_2$ ), scan frequency ( $N_3$ , Hz), course angle ( $N_4$ , °), aspect angle ( $N_5$ , °), and height ( $N_6$ , m), while response variable is a 3D coordinate error ( $N_1, N_2, N_3, \dots, N_6$  are the serial numbers of the six design variable parameters).

### Data analysis

Experimental data were fitted to a second-order polynomial model.<sup>58</sup> The generalized second-order polynomial model used in the response surface analysis is as follows

$$F = \beta_0 + \sum_{i=1}^6 \beta_i N_i + \sum_{i=1}^6 \beta_{ii} N_i^2 + \sum_{i/j=1}^6 \beta_{ij} N_i N_j \quad (3)$$

where  $\beta_0$ ,  $\beta_i$ ,  $\beta_{ii}$ , and  $\beta_{ij}$  are the regression coefficients for intercept, linear, quadratic, and interaction terms, respectively, and  $N_i$  and  $N_j$  are the independent variable parameters. The independent parameters and their response variables are used to establish the response surfaces and contour plots while holding a variable parameter constant in the second-order polynomial model. When the results showed a saddle point in response surfaces, the estimated ridge of the optimum response can be computed.

Optimal conditions for the accurate scanning of airborne scanner depend on speed, ground feature, scan frequency, course angle, aspect angle, and height which

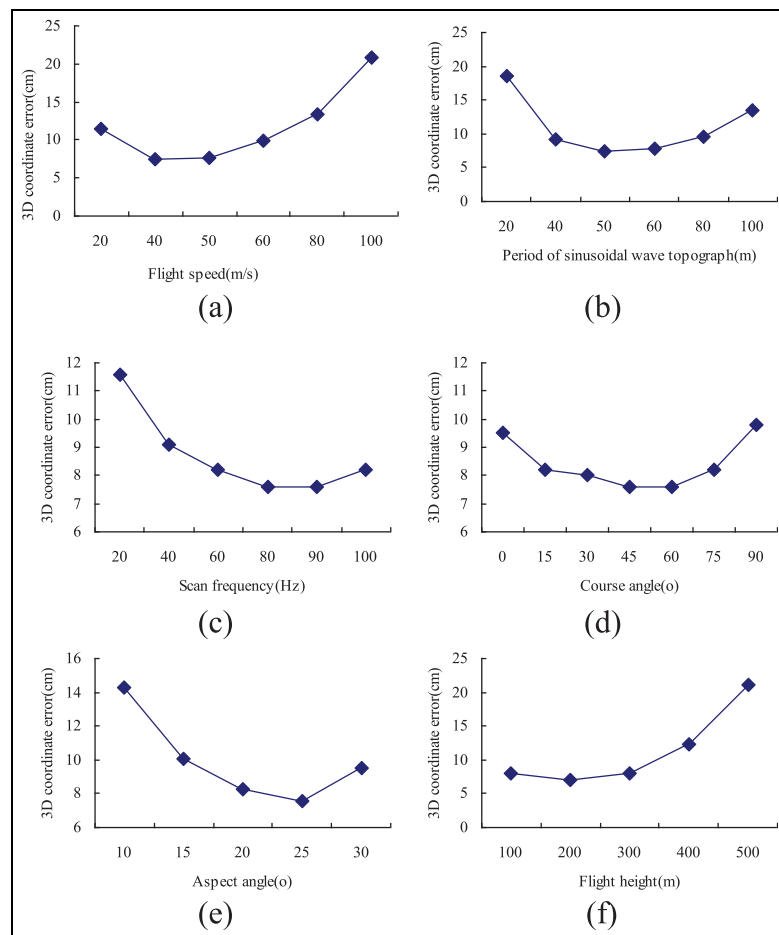


**Figure 3.** Impacts of parameters on measurement accuracy of airborne scanner: (a) flight speed, (b) period of sinusoidal wave topography, (c) scan frequency, (d) course angle, (e) aspect angle, and (f) flight height.

were all obtained by using the predictive equations from RSM. The total 3D coordinate error in measurement is estimated with optimal working parameters in the airborne scanner. The experimental and predicted values are compared with the results in order to validate the model.

## Results and discussion

### Analysis of preliminary experimental results

The results of the preliminary experiment are shown in Figure 3.

**The influence of flight speed.** In this group of experiments, the actual value of sinusoidal wave period is 50 s, scan frequency is 75 Hz, course angle is 45°, aspect angle is 20°, and flight height is 300 m. These are all constant. It can be known from Figure 3(a) that the curve of 3D coordinate error has three stages. Stage 1 is the period before the flight speed up to 40 m/s where the 3D coordinate error decreases with flight speed up. Stage 2 is the period when flight speed up from 40 to 50 m/s where the 3D coordinate error does not show

significant changes. Stage 3 is the period when flight speed is more than 50 m/s. The 3D coordinate error starts to increase dramatically. Results indicated that when the flight speed ranges from 40 to 50 m/s, the measurement accuracy of airborne scanner can be controlled within a small bound.

**The influence of ground feature.** Period of sinusoidal wave topography is the parameter of ground feature. In this group of experiments, the flight speed is set at 60 m/s, scan frequency is set at 75 Hz, course angle is set at 45°, aspect angle is set at 20°, and flight height is set at 300 m. The change law between period of sinusoidal wave and 3D coordinate error is shown in Figure 3(b). It shows that the 3D coordinate error decreases with increasing period of sinusoidal wave topography up to 50 m and then begins to increase with increasing period of sinusoidal wave topography. The reason is that when the amplitude of sinusoidal wave topography is constant, the larger the period of sinusoidal wave topography is, the flatter the ground surface is. A large scan area in one period of sinusoidal wave will affect the measurement accuracy. Results indicate that when the

**Table 1.** Independent parameters and their actual values used for optimization.

Serial number	Independent variable parameter	Units	Symbol	Level		
				-1	0	1
$N_1$	Flight speed	m/s	A	20	60	100
$N_2$	Ground feature	type	B	1	2	3
$N_3$	Scan frequency	Hz	C	50	75	100
$N_4$	Course angle	°	D	0	45	90
$N_5$	Aspect angle	°	E	10	20	30
$N_6$	Flight height	m	F	100	300	500

amplitude of sinusoidal wave topography is 5 m, the best ground feature for measurement is that the period of sinusoidal wave topography is close to 50 m.

**The influence of scan frequency.** In this group of experiments, the flight speed is set at 60 m/s, sinusoidal wave period is set at 50 m, course angle is set at 45°, aspect angle is set at 20°, and flight height is set at 300 m. It can be seen from Figure 3(c) that the curve of 3D coordinate error has three stages: Stage 1 is the period before the scan frequency up to 80 Hz where the 3D coordinate error decreases with increasing of scan frequency; Stage 2 is the period when scan frequency changes from 80 to 90 Hz while the 3D coordinate error is almost unchanging; and Stage 3 is the period when scan frequency is more than 90 Hz, the 3D coordinate error starts to increase slowly. Results indicated that when the scan frequency ranges from 80 to 90 Hz, the measurement accuracy of airborne scanner is the best.

**The influence of course angle.** In this group of experiments, the actual values of flight speed of 60 m/s, sinusoidal wave period of 50 m, scan frequency of 75 Hz, aspect angle of 20°, and flight height of 300 m are all constant. The change law between course angle and 3D coordinate error is shown in Figure 3(d). It shows that the curve of 3D coordinate error has three stages: Stage 1 is the period before the course angle up to 45° where the 3D coordinate error declines with increasing of course angle, and the decline rate is gradually decreasing; Stage 2 is the period when course angle up from 45° to 60° where the 3D coordinate error is nearly constant; Stage 3 is the period when course angle is more than 60°, the 3D coordinate error begins to increase and the change rate is gradually increasing. Results indicated that the best course angle for the measurement of airborne scanner ranges from 45° to 60°.

**The influence of aspect angle.** In this group of experiments, the flight speed is set at 60 m/s, sinusoidal wave period is set at 50 m, scan frequency is set at 75 Hz, course angle is set at 45°, and flight height is set at 300 m. The change law between aspect angle and 3D coordinate error is shown in Figure 3(e). It shows that

before the aspect angle increases up to 25°, the 3D coordinate error decreases with increasing of aspect angle. When the aspect angle increases to a value more than 25°, the 3D coordinate error starts to increase with increasing of aspect angle. The reason is that when the height of scanner is constant, the larger the aspect angle, the farther the distance between the measure point and scanner lens is. Thus, the measurement accuracy will be affected accordingly. Results indicate that the best aspect angle for measurement in this experiment is close to 25°.

**The influence of flight height.** In this group of experiments, the flight speed is set at 60 m/s, sinusoidal wave period is set at 50 m, scan frequency is set at 75 Hz, course angle is set at 45°, and aspect angle is set at 20°. The change law between flight height of unmanned aircraft and 3D coordinate error is shown in Figure 3(f). It shows that the 3D coordinate error increases with the increasing of flight height. The main reason is the increasing travel distance of the scanning beam from emitter to scan point. It may be more seriously disturbed and interrupted in the process of measurement. Figure 3(f) also indicates that when the flight height is less than 300 m, the 3D coordinate error will not change too much anymore.

### Results of main experiment

Based on the preliminary experiment, the independent variable parameters and their actual values used for optimization are determined and showed in Table 1, in which the level “-1” of ground feature indicates that the ground surface is approximately a sinusoidal wave topography with period of 20 m and amplitude of 5 m. The level “0” of ground feature indicates that the ground surface is approximately a sinusoidal wave topography with period of 50 m and amplitude of 5 m, and the level “1” indicates a sinusoidal wave topography with period of 80 m and amplitude of 5 m.

The detailed value of the six parameters in the experiments designed for RSM and the values of response variable (3D coordinate error) are shown in Table 2.

**Table 2.** The experimental results of RSM.

No.	Independent variable parameter						Response variable			
	A Speed (m/s)	B Ground feature	C Scan frequency (Hz)	D Course angle (°)	E Aspect angle (°)	F Height (m)	$\Delta x$ (cm)	$\Delta y$ (cm)	$\Delta z$ (cm)	3D coordinate error (cm)
1	60	2	75	45	20	300	3.13	1.62	6.13	7.07
2	20	1	75	0	20	300	10.12	4.27	10.35	15.09
3	60	1	100	45	10	300	17.14	12.79	19.51	28.95
4	60	2	50	0	20	100	10.83	3.40	5.67	12.69
5	60	3	100	45	30	300	7.11	0.59	13.25	15.05
6	60	1	75	45	30	100	10.67	3.68	6.47	13.01
7	100	3	75	90	20	300	9.88	2.61	13.27	16.75
8	100	1	75	90	20	300	19.93	15.39	22.80	33.97
9	60	3	100	45	10	300	11.95	6.18	7.09	15.21
10	60	3	75	45	30	100	8.65	6.97	23.65	26.13
11	60	1	75	45	30	500	10.22	11.25	21.72	26.51
12	20	3	75	90	20	300	4.74	5.23	11.06	13.12
13	60	2	75	45	20	300	4.23	2.81	4.15	6.56
14	20	1	75	90	20	300	11.62	9.60	7.79	16.97
15	100	3	75	0	20	300	13.89	7.29	20.36	25.70
16	100	2	75	90	10	300	16.52	11.67	17.72	26.89
17	60	1	75	45	10	100	13.96	12.05	12.31	22.17
18	100	2	100	45	20	100	8.10	9.12	10.95	16.39
19	60	1	100	45	30	300	12.01	7.95	9.27	17.13
20	60	1	50	45	30	300	22.74	13.86	15.69	30.91
21	100	2	75	90	30	300	15.07	11.30	14.08	23.52
22	100	2	50	45	20	100	9.25	6.17	9.45	14.59
23	20	2	100	45	20	100	5.21	7.09	8.32	12.11
24	60	2	75	45	20	300	4.29	6.52	7.14	10.58
25	60	2	100	90	20	500	10.93	11.55	17.26	23.47
26	20	3	75	0	20	300	9.66	9.24	18.96	23.20
27	20	2	100	45	20	500	14.51	3.68	17.38	22.94
28	60	2	75	45	20	300	6.62	5.30	6.97	10.98
29	60	3	75	45	10	100	2.47	9.96	20.93	23.31
30	20	2	75	90	10	300	13.60	7.38	16.18	22.39
31	20	2	50	45	20	500	15.98	9.06	20.57	27.58
32	60	1	75	45	10	500	19.47	21.19	22.24	36.37
33	60	2	50	0	20	500	10.25	7.08	6.75	14.17
34	100	1	75	0	20	300	21.40	19.74	16.23	33.33
35	60	3	75	45	10	500	9.14	9.21	19.51	23.43
36	100	2	100	45	20	500	17.12	11.60	15.96	26.12
37	60	2	50	90	20	500	17.37	10.19	14.63	24.89
38	60	2	75	45	20	300	1.34	5.23	4.81	7.23
39	20	2	50	45	20	100	10.28	6.10	9.52	15.28
40	60	2	50	90	20	100	10.69	2.87	7.03	13.11
41	60	3	50	45	10	300	5.23	7.65	11.32	14.63
42	100	2	75	0	10	300	12.10	8.91	18.74	24.02
43	20	2	75	0	30	300	4.73	6.39	6.95	10.56
44	60	2	100	90	20	100	5.91	7.25	9.14	13.08
45	20	2	75	90	30	300	7.19	7.06	9.53	13.87
46	100	2	75	0	30	300	14.33	9.18	13.69	21.84
47	60	2	100	0	20	500	13.55	10.03	12.17	20.79
48	60	3	50	45	30	300	6.83	8.24	11.02	15.36
49	60	3	75	45	30	500	12.17	3.57	16.60	20.89
50	60	2	100	0	20	100	6.80	6.48	9.21	13.15
51	100	2	50	45	20	500	16.53	15.72	26.58	35.03
52	20	2	75	0	10	300	7.84	8.07	10.12	15.13
53	60	1	50	45	10	300	16.79	13.65	17.73	27.97

RSM: response surface method; 3D coordinate error: three-dimensional coordinate error.

Table 2 shows that when the values of speed change from 20 to 100 m/s, period of sinusoidal wave topography (ground feature) changes from 50 to 100 m, scan frequency ranges from 20 to 100 Hz, course angle

changes from 0° to 90°, aspect angle changes from 10° to 30°, height changes from 100 to 500 m, and the maximum experimental values of  $\Delta x$ ,  $\Delta y$ , and  $\Delta z$  are 22.74, 21.19, and 26.58 cm, respectively. The minimum



**Table 3.** The verification index of experimental results of RSM.

Source	Sum of squares	Degrees of freedom	Mean square	F-value	P-value	
Model <sup>a</sup>	2505.94	27	92.81	5.44	< 0.0001	Significant
A—Speed	336.90	1	336.90	19.76	0.0002	
B—Ground feature	201.74	1	201.74	11.83	0.0021	
C—Scan frequency	19.87	1	19.87	1.17	0.2907	
D—Course angle	6.36	1	6.36	0.37	0.5469	
E—Aspect angle	86.98	1	86.98	5.10	0.0329	
F—Height	478.29	1	478.29	28.05	< 0.0001	
AB	105.9	1	105.90	6.21	0.0197	
AC	0.061	1	0.061	0.0036	0.9527	
AD	2.34	1	2.34	0.14	0.7144	
AE	7.11	1	7.11	0.42	0.5244	
AF	6.18	1	6.18	0.36	0.5525	
BC	21.33	1	21.33	1.25	0.2740	
BD	58.03	1	58.03	3.40	0.0769	
BE	51.64	1	51.64	3.03	0.0941	
BF	134.59	1	134.59	7.89	0.0095	
CD	9.1	1	9.10	0.53	0.4718	
CE	30.56	1	30.56	1.79	0.1927	
CF	3.44	1	3.44	0.20	0.6571	
DE	3.30	1	3.30	0.19	0.6636	
DF	21.30	1	21.30	1.25	0.2743	
EF	4.58	1	4.58	0.27	0.6088	
A <sup>2</sup>	338.41	1	338.41	19.85	0.0002	
B <sup>2</sup>	409.29	1	409.29	24.00	< 0.0001	
C <sup>2</sup>	32.04	1	32.04	1.88	0.1826	
D <sup>2</sup>	22.54	1	22.54	1.32	0.2611	
E <sup>2</sup>	153.78	1	153.78	9.02	0.0060	
F <sup>2</sup>	260.55	1	260.55	15.28	0.0006	
Residual	426.26	25	17.05	—	—	
Lack of fit	408.38	21	19.45	4.35	0.0815	Not significant
Pure error	17.88	4	4.47	—	—	

RSM: response surface method.

<sup>a</sup>R<sup>2</sup> = 0.907.

experimental values of  $\Delta x$ ,  $\Delta y$ , and  $\Delta z$  are 1.34, 0.59, and 4.15 cm, respectively. The 3D coordinate error ranges from 6.56 to 36.37 cm.

### Efficiency evaluation of response surfaces

The verification index of the experimental results is calculated and shown in Table 3. In Table 3, the “Model *F*-value” of 5.44 and “Lack of Fit *F*-value” of 4.35 imply that the model is significant and the influence of different parameters on the 3D coordinate error can be well described by the response surface model. The “Model *P*-value” of 0.0001 and “Lack of Fit *P*-value” of 0.0815 imply that there is only 0.01% chance that the model could fail and only 8.15% chance that the model is lack of fit. The coefficient of determination is 0.907 (*R*<sup>2</sup>), which indicates the regression model is performing well.

### Evaluation and optimization of independent parameters

In Table 3, “*P*-value” indicates the influence of independent parameters on 3D coordinate errors. The smaller the value is, the higher the influence is. Thus, it

can be concluded from Table 3 that the parameters can be ordered by their influences as flight height, flight speed, ground feature, aspect angle, scan frequency, and course angle.

*P*-value less than 0.05 indicates that model terms are significant. In this case, parameters *A*, *B*, *E*, and *F* are significant model terms, which indicate that flight speed, ground feature, aspect angle, and flight height are the parameters which can significantly influence the 3D coordinate error in measurement. Values greater than 0.10 indicate that the model terms are not significant. Thus, both the scan frequency and course angle are not the significant parameters.

According to the generalized second-order polynomial model and experimental results, the response surfaces of interaction between different independent parameters on 3D coordinate error of measurement are drawn in Figures 4 to 18.

Figure 4 shows the effects of flight speed and ground feature on 3D coordinate error of measurement accuracy. In this response surface, the actual value of scan frequency is 75 Hz, course angle is 45°, aspect angle is 20°, and flight height is 300 m. When the ground feature is constant, the 3D coordinate error decreases with the speed before the speed up to 46.14 m/s, and after

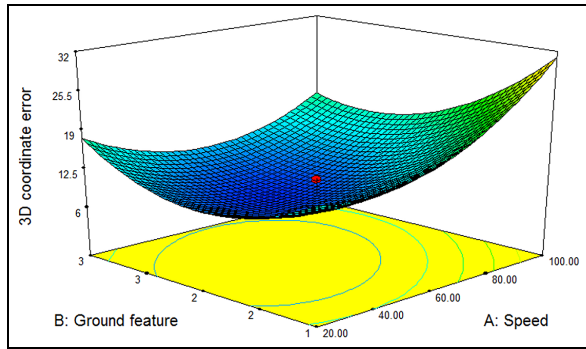


**Figure 4.** Response surface for the effects of flight speed and ground feature on 3D coordinate error.

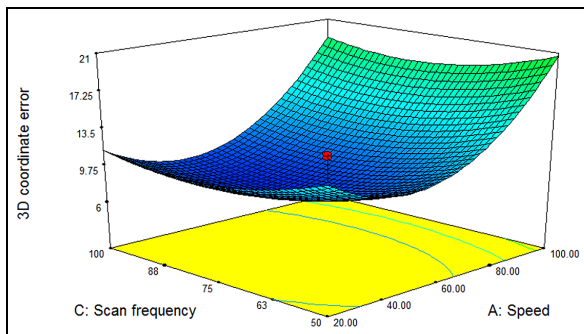
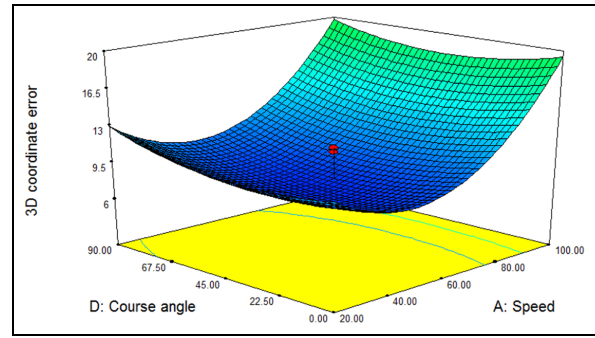


**Figure 5.** Response surface for the effects of flight speed and scan frequency on 3D coordinate error.

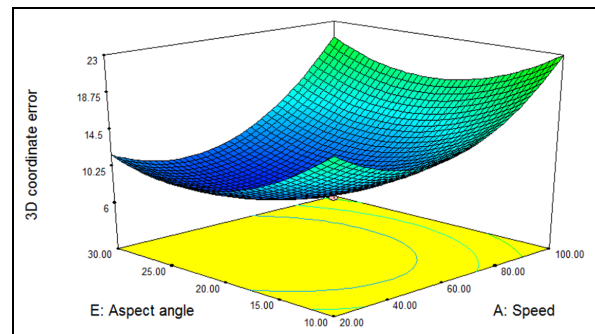
that the 3D coordinate error increases with the speed. Similarly, when the speed is constant, the 3D coordinate error decreases at first and then increases with ground feature. The optimum values of speed and ground feature are 46.14 m/s and type 2. Moreover, a value of 0.0197 for “*AB P-value*” (Table 3) indicates that the interaction between flight speed and ground feature is significant on 3D coordinate error.

Figure 5 shows the effects of flight speed and scan frequency on 3D coordinate error of measurement accuracy. In this response surface, the actual value of ground feature is type 2, course angle is 45°, aspect angle is 20°, and flight height is 300 m. When the scan frequency is constant, the 3D coordinate error decreases with the speed before the speed up to 46.14 m/s. After that, the 3D coordinate error increases with the speed. When the speed is constant, the 3D coordinate error slowly decreases before the scan frequency up to 88 Hz and then increases very slowly. The optimum values of speed and scan frequency are 46.14 m/s and 88 Hz. Moreover, a value of 0.9527 for “*AC P-value*” (Table 3) indicates that the interaction between flight speed and scan frequency is not significant on 3D coordinate error.

Figure 6 shows the effects of flight speed and course angle on 3D coordinate error of measurement accuracy. In this response surface, the actual value of ground



**Figure 6.** Response surface for the effects of flight speed and course angle on 3D coordinate error.

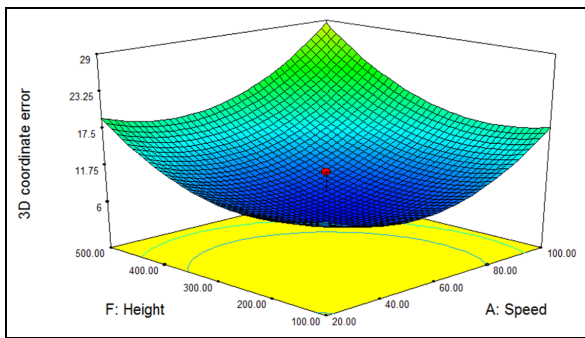


**Figure 7.** Response surface for the effects of flight speed and aspect angle on 3D coordinate error.

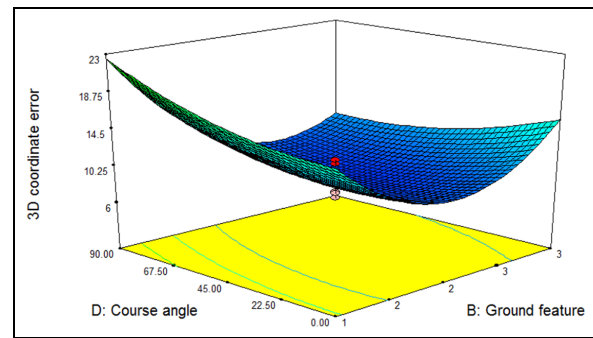
feature is type 2, scan frequency is 75 Hz, aspect angle is 20°, and flight height is 300 m. When the course angle is constant, the 3D coordinate error decreases with the speed before the speed up to 46.14 m/s, and after that the 3D coordinate error increases with the speed. Similarly, when the course angle is constant, the 3D coordinate error slowly decreases at first and then slowly increases with course angle. The optimum values of speed and course angle are 46.14 m/s and 54.4°. Moreover, a value of 0.7144 for “*AD P-value*” (Table 3) indicates that the interaction between flight speed and course angle is not significant on 3D coordinate error.

Figure 7 shows the effects of flight speed and aspect angle on 3D coordinate error of measurement accuracy. In this response surface, the actual value of ground feature is type 2, scan frequency is 75 Hz, course angle is 45°, and flight height is 300 m. When the speed is constant, the 3D coordinate error slowly decreases with the aspect angle before the aspect angle up to 24.12°, and after that the 3D coordinate error increases. Similarly, when the aspect angle is constant, the 3D coordinate error decreases at first and then increases with speed. The optimum values of speed and aspect angle are 46.14 m/s and 24.12°.

Figure 8 shows the effects of flight speed and flight height on 3D coordinate error of measurement



**Figure 8.** Response surface for the effects of flight speed and flight height on 3D coordinate error.



**Figure 10.** Response surface for the effects of ground feature and course angle on 3D coordinate error.

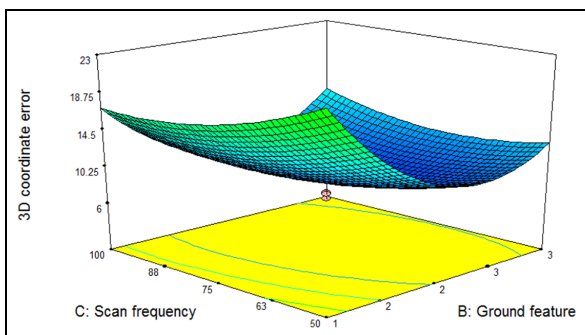


**Figure 9.** Response surface for the effects of ground feature and scan frequency on 3D coordinate error.

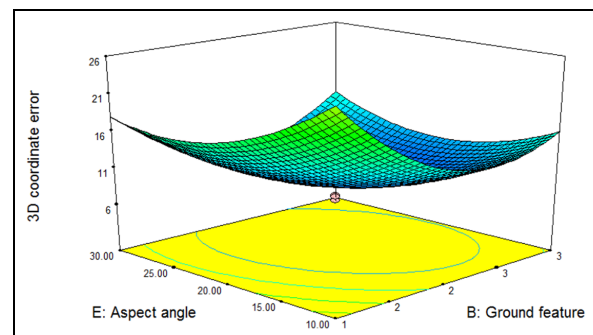


**Figure 11.** Response surface for the effects of ground feature and aspect angle on 3D coordinate error.

accuracy. In this response surface, the actual values of ground feature of type 2, scan frequency of 75 Hz, course angle of  $45^\circ$ , and aspect angle of  $20^\circ$  are all constant. When the speed is constant, the 3D coordinate error decreases with flight height before the flight height up to 215.92 m, and after that the 3D coordinate error increases. Similarly, when the height is constant, the 3D coordinate error decreases at first and then increases with speed. The optimum values of speed and height are 46.14 m/s and 215.92 m, respectively.

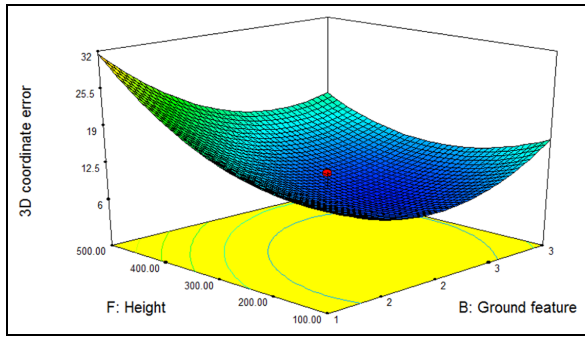
Figure 9 shows the effects of ground feature and scan frequency on 3D coordinate error of measurement accuracy. In this response surface, the actual values of flight speed of 60 m/s, course angle of  $45^\circ$ , aspect angle of  $20^\circ$ , and flight height of 300 m are all constant. When the ground feature is constant, the 3D coordinate error decreases with the scan frequency before the scan frequency up to 88 Hz, and after that the 3D coordinate error increases. Similarly, when the scan frequency is constant, the 3D coordinate error decreases at first and then increases with ground feature. The optimum values of ground feature and scan frequency are type 2 and 88 Hz, respectively.

Figure 10 shows the effects of ground feature and course angle on 3D coordinate error of measurement accuracy. In this response surface, the actual value of flight speed is 60 m/s, scan frequency is 75 Hz, aspect angle is  $20^\circ$ , and flight height is 300 m. When the

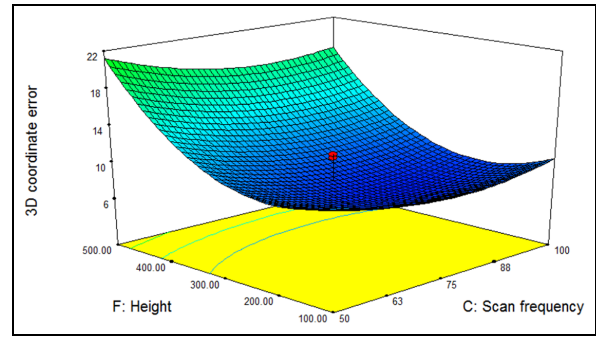
ground feature is constant, the 3D coordinate error decreases with course angle before the course angle up to  $54.4^\circ$ , and after that the 3D coordinate error increases. Similarly, when the course angle is constant, the 3D coordinate error decreases at first and then increases with ground feature. The optimum values of ground feature and course angle are type 2 and  $54.4^\circ$ .

Figure 11 shows the effects of ground feature and aspect angle on 3D coordinate error of measurement accuracy. In this response surface, the actual values of flight speed of 60 m/s, scan frequency of 75 Hz, course angle of  $45^\circ$ , and flight height of 300 m are all constant. When the ground feature is constant, the 3D coordinate error decreases slowly with aspect angle before the aspect angle up to  $24.12^\circ$ , and after that the 3D coordinate error increases. Similarly, when the aspect angle is constant, the 3D coordinate error decreases at first and then increases with ground feature. The optimum values of ground feature and aspect angle are type 2 and  $24.12^\circ$ .

Figure 12 shows the effects of ground feature and flight height on 3D coordinate error of measurement accuracy. In this response surface, the actual value of flight speed is 60 m/s, scan frequency is 75 Hz, course angle is  $45^\circ$ , and aspect angle is  $20^\circ$ . When the ground feature is constant, the 3D coordinate error decreases with height before the height up to 215.92 m, and after that the 3D coordinate error increases. Similarly, when



**Figure 12.** Response surface for the effects of ground feature and flight height on 3D coordinate error.



**Figure 15.** Response surface for the effects of scan frequency and flight height on 3D coordinate error.

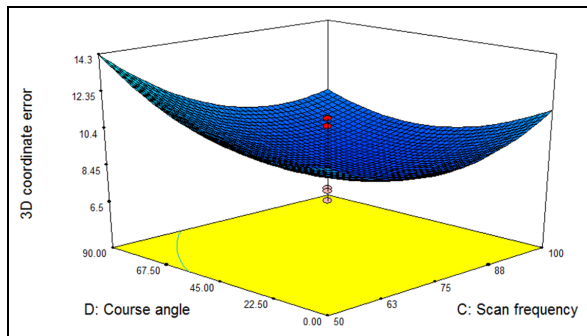


**Figure 13.** Response surface for the effects of scan frequency and course angle on 3D coordinate error.

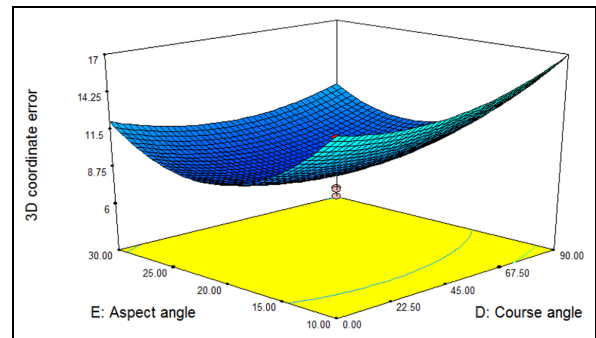


**Figure 16.** Response surface for the effects of course angle and aspect angle on 3D coordinate error.

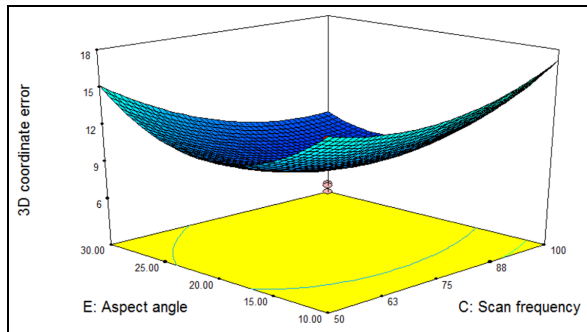


**Figure 14.** Response surface for the effects of scan frequency and aspect angle on 3D coordinate error.

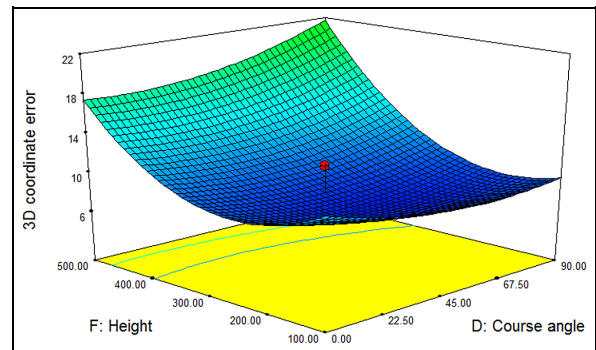


**Figure 17.** Response surface for the effects of course angle and flight height on 3D coordinate error.

the height is constant, the 3D coordinate error decreases at first and then increases with ground feature. The optimum values of ground feature and height are type 2 and 215.92m, respectively. Moreover, a value of 0.0095 for “BF P-value” (Table 3) indicates that the interaction between ground feature and flight height is significant on 3D coordinate error.

Figures 13–15 show the interaction effects of “scan frequency and course angle,” “scan frequency and aspect angle,” and “scan frequency and flight height” on 3D coordinate error of measurement accuracy, respectively. In Figure 13, the actual value of flight

speed is 60 m/s, ground feature is type 2, aspect angle is 20°, and flight height is 300 m. In Figure 14, the actual value of flight speed is 60 m/s, ground feature is type 2, and flight height is 300 m. In Figure 15, the actual values of flight speed of 60 m/s, ground feature of type 2, course angle of 45°, and aspect angle of 20° are all constant. It can be concluded from Figures 13 to 15 that the optimum values of scan frequency, course angle, aspect angle, and height are 88 Hz, 54.40°, 24.12°, and 215.92 m, respectively.

Figures 16–18 show the interaction effects of “course angle and aspect angle,” “course angle and

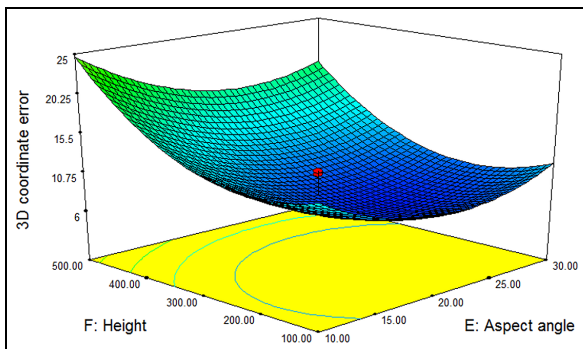


**Figure 18.** Response surface for the effects of aspect angle and flight height on 3D coordinate error.

flight height,” and “aspect angle and flight height” on 3D coordinate error of measurement accuracy. In Figure 16, the actual value of flight speed is 60 m/s, ground feature is type 2, scan frequency is 75 Hz, and flight height is 300 m. In Figure 17, the actual value of flight speed is 60 m/s, ground feature is type 2, scan frequency is 75 Hz, and aspect angle is 20°. In Figure 18, the actual value of flight speed is 60 m/s, ground feature is type 2, scan frequency is 75 Hz, and course angle is 45°. It can be concluded from Figures 16 to 18 that the optimum values of course angle, aspect angle, and height are 54.40°, 24.12°, and 215.92 m, respectively.

The slope of surfaces reflects the effects of interactions on two different variable parameters on response values. Therefore, it can be known from the shape of response surfaces that the top three heavily influenced interactions on 3D coordinate error are “Ground feature and Height,” “Speed and Ground feature,” and “Ground feature and Course angle.”

By substituting different groups of independent parameter and their response variable into equation (3), the generalized second-order polynomial model of these experiments can be written as

$$\begin{aligned}
 S = & 8.49 + 3.75A - 2.90B - 0.91C + 0.51D \\
 & - 1.90E + 4.46F - 3.64AB + 0.087AC \\
 & - 0.38AD + 0.94AE \\
 & + 0.88AF + 1.63BC - 2.69BD + 1.8BE - 4.1BF \\
 & - 1.07CD - 1.95CE - 0.46CF - 0.64DE + 1.63DF \\
 & - 0.76EF + 5.84A^2 + 6.43B^2 + 1.8C^2 + 1.51D^2 \\
 & + 3.94E^2 + 5.13F^2
 \end{aligned} \quad (4)$$

where  $S$  is the value of response variable (3D coordinate error) and  $A$ ,  $B$ ,  $C$ ,  $D$ ,  $E$ , and  $F$  are the parameters of flight speed, ground feature, scan frequency, course angle, aspect angle, and flight height, respectively. By taking the partial derivatives of each response variable parameter, equation (4) can be solved and the predicted optimum values of parameters are flight speed of 46.14 m/s, ground feature of type 2, scan frequency of

88 Hz, course angle of 54.4°, aspect angle of 24.12°, and flight height of 215.92 m. The predicted optimum values from calculations are the same with the analyses of response surface. The predicted optimum value of response variable is 6.45 cm.

### Verification experiments

Verification experiments performed three times at the predicted optimum conditions (value of variable parameters) derived from analysis by RSM. The average result (minimum 3D coordinate error) in verification experiments is 5.97 cm while the predicted value is 6.45 cm. It can be concluded that experimental values are reasonably close to the predicted values, confirming the validity and adequacy of the predicted models. The verification experiments showed that the predicted values from the RSM are quite close to the experimental values, which validate the proposed approach.

### Conclusion

In this paper, the working parameters affecting the measurement accuracy of airborne scanner are evaluated by using the RSM. The results showed that the second-order polynomial model could be used to optimize the use of working parameters for minimizing the 3D coordinate errors. Flight height is found to be the most influencing parameter in measurement accuracy of airborne scanner. Based on the analysis, the optimum values of working parameters for minimizing the 3D coordinate errors are flight speed of 46.14 m/s, ground feature of type 2, scan frequency of 88 Hz, course angle of 54.4°, aspect angle of 24.12°, and flight height of 215.92 m. Under optimized conditions, the experimental values agreed well with the values predicted by response surface models. The results from this study could be used as a reference for engineers to conduct airborne scanner-based measurement.

### Acknowledgements

The data used to support the findings of this study are available from the corresponding author upon request.


### Declaration of conflicting interests

The author(s) declared no potential conflicts of interest with respect to the research, authorship, and/or publication of this article.

### Funding

This study was financially supported by the Education and Teaching Foundation of Hubei Province (2017GB070), Science and Technology Innovation Team Foundation of Hubei Province Education Department (T201823), and Construction Science and Technology Foundation of Hubei Province (2017 A16).

## ORCID iD

Yi Zhang  <https://orcid.org/0000-0002-1113-8465>

## References

- Persson A. Detecting and measuring individual trees using an airborne laser scanner. *Photogramm Eng Remote Sens* 2002; 68(9): 925–932.
- Yang H, Omidalizrandi M, Xu X, et al. Terrestrial laser scanning technology for deformation monitoring and surface modeling of arch structures. *Compos Struct* 2017; 169: 173–179.
- Holmgren J and Persson Å. Identifying species of individual trees using airborne laser scanner. *Remote Sens Environ* 2004; 90(4): 415–423.
- Yang H, Xu X, Xu W, et al. Terrestrial laser scanning-based deformation analysis for arch and beam structures. *IEEE Sens J* 2017; 17: 4605–4611.
- Shui L, Chen F, Garg A, et al. Design optimization of battery pack enclosure for electric vehicle. *Struct Multidiscip O* 2018; 58(1): 331–347.
- Garg A, Shankhwar K, Jiang D, et al. An evolutionary framework in modelling of multi-output characteristics of the bone drilling process. *Neural Comput Appl* 2018; 29(11): 1233–1241.
- Rottensteiner F, Trinder J, Clode S, et al. Building detection by fusion of airborne laser scanner data and multi-spectral images: performance evaluation and sensitivity analysis. *ISPRS J Photogramm Remote Sens* 2007; 62(2): 135–149.
- Stal C, Tack F, Maeyer PD, et al. Airborne photogrammetry and LiDAR for DSM extraction and 3D change detection over an urban area—a comparative study. *Int J Remote Sens* 2013; 34(4): 1087–1110.
- Zhang DB, Zhang Y, Cheng T, et al. Measurement of displacement for open pit to underground mining transition using digital photogrammetry. *Measurement* 2017; 109(10): 187–199.
- Fei W. Theoretical analysis of influence of laser signal strength on range precision in single photon ranging. *Acta Optica Sinica* 2010; 30(10): 2771–2775.
- Xu X, Yang H and Neumann I. Time-efficient filtering method for three-dimensional point clouds data of tunnel structures. *Adv Mech Eng* 2018; 10: 1–6.
- Xu X, Yang H, Zhang Y, et al. Intelligent 3D data extraction method for deformation analysis of composite structures. *Compos Struct* 2018; 203: 254–258.
- Kobler A, Pfeifer N, Ogrinc P, et al. Repetitive interpolation: a robust algorithm for DTM generation from aerial laser scanner data in forested terrain. *Remote Sens Environ* 2007; 108(1): 9–23.
- Mikita T, Klimánek M and Cibulka M. Evaluation of interpolation methods of airborne laser scanning data for detection of trees and their heights. *Zprávy Lesnického Výzkumu* 2013; 58(2): 99–106.
- Jian-Wei WU and Hong-Chao MA. Error analysis on laser beam misalignment with scanner mirror of airborne LiDAR. *Infrared Laser Eng* 2008; 37(2): 243–246.
- Zhang DB, Zhang Y and Cheng T. Measurement of grass root reinforcement for copper slag mixed soil using improved shear test apparatus and calculating formulas. *Measurement* 2018; 118(10): 14–22.
- Muthukumar V, Rajesh N, Venkatasamy R, et al. Mathematical modeling for radial overcut on electrical discharge machining of Incoloy 800 by response surface methodology. *Procedia Mater Science* 2014; 6: 1674–1682.
- Emamdjomeh Z, Shamaei S and Moini S. Modeling and optimization of ultrasound assisted osmotic dehydration of cranberry using response surface methodology. *J Agric Sci Tech* 2018; 14(3): 1523–1534.
- Yang H, Xu X, Kargoll B, et al. An automatic and intelligent optimal surface modeling method for composite tunnel structures. *Compos Struct* 2018; 208: 702–710.
- Garg A, Peng X, Le MLP, et al. Design and analysis of capacity models for Lithium-ion battery. *Measurement* 2018; 120: 114–120.
- Zhang Y, Kim CW, Beer M, et al. Modeling multivariate ocean data using asymmetric copulas. *Coastal Eng* 2018; 135: 91–111.
- Zhang Y. Investigating dependencies among oil price and tanker market variables by copula-based multivariate models. *Energy* 2018; 161: 435–466.
- Zhang Y, Kim CW, Tee KF, et al. Long-term health monitoring for deteriorated bridge structures based on Copula theory. *Smart Struct Syst* 2018; 21(2): 171–185.
- Soderman U, Ahlberg S, Elmqvist M, et al. Three-dimensional environment models from airborne laser radar data. *Proc SPIE* 2004; 5412: 333–344.
- Steinval OK, Soederman U and Letalick D. Airborne laser radar: systems and methods for reconnaissance and terrain modeling. *Proc SPIE* 1999; 3707: 12–26.
- Filin S. Recovery of systematic biases in laser altimetry data using natural surfaces. *Photogramm Eng Remote Sens* 2003; 69(11): 1235–1242.
- Wang J, Xu L, Li X, et al. Quantitative evaluation of impacts of random errors on ALS accuracy using multiple linear regression method. *IEEE Trans Instrument Measure* 2012; 61(8): 2242–2252.
- Imai M, Sakamoto H and Sakata M. Vehicle attitude angle calculating device, and lane departure warning system using same. US9123110B2, 2015.
- Maltamo M, Mustonen K, Hyypä J, et al. The accuracy of estimating individual tree variables with airborne laser scanning in a boreal nature reserve. *Revue Canadienne Recherche Forestière* 2004; 34(9): 1791–1801.
- Holopainen M, Mäkinen A, Rasinmäki J, et al. Effect of tree-level airborne laser-scanning measurement accuracy on the timing and expected value of harvest decisions. *Eur J Forest Res* 2010; 129(5): 899–907.
- Wang J, Xu L, Li X, et al. Impact analysis of random measurement errors on airborne laser scanning accuracy. *Instrument Measure Tech Conf* 2011; 78: 1–4.
- Wang J, Xu L, Li X, et al. Quantitatively evaluating random attitude measurement errors' impacts on DSM elevation accuracy from airborne laser scanning. *IEEE Trans Instrument Measure* 2013; 62(11): 3101–3109.
- Wu B, Han S, Xiao J, et al. Error compensation based on BP neural network for airborne laser ranging. *Int J Light Electron Optics* 2016; 127(8): 4083–4088.
- Næsset E. Influence of terrain model smoothing and flight and sensor configurations on detection of small pioneer trees in the boreal–alpine transition zone utilizing height metrics derived from airborne scanning lasers. *Remote Sens Environ* 2009; 113(10): 2210–2223.

35. Goodwin NR, Coops NC and Culvenor DS. Assessment of forest structure with airborne LiDAR and the effects of platform altitude. *Remote Sens Environ* 2006; 103(2): 140–152.
36. Watt MS, Meredith A, Watt P, et al. The influence of LiDAR pulse density on the precision of inventory metrics in young unthinned Douglas-fir stands during initial and subsequent LiDAR acquisitions. *New Zealand J Forest Sci* 2014; 44(1): 1–9.
37. Wang J, Xu L, Li X, et al. Impact of attitude deviations on laser point cloud of airborne LiDAR. *Chin J Sci Instrument* 2011; 32(8): 1810–1817.
38. Zhang Y, Gomes A, Beer M, et al. Reliability analysis with consideration of asymmetrically dependent variables: discussion and application to geotechnical examples. *Reliabil Eng Syst Safety* 2018; 185: 261–277.
39. Box GEP and Wilson KB. On the experimental attainment of optimum conditions. *J Royal Statist Soc* 1951; 13(1): 1–45.
40. Bowerman BL. Statistical design and analysis of experiments: with applications to engineering and science, second edition. *Technometrics* 2003; 33(1): 105–106.
41. Yang P, Tan X, Sun H, et al. Fire accident reconstruction based on les field model by using orthogonal experimental design method. *Adv Eng Software* 2011; 42(11): 954–962.
42. Patel B and Rathod KB. *Application of response surface methodology*. Lap Lambert Academic Publishing, 2012. Brivibas gatve 197, LV-1039, Riga, Latvia, European Union.
43. Mohammed BS and Adamu M. Evaluating the static and dynamic modulus of elasticity of roller compacted rubbercrete using response surface methodology. *Int J Geomate* 2018; 14(41): 186–192.
44. Khuri AI and Mukhopadhyay S. Response surface methodology. *Wiley Interdis Rev Comput Stat* 2010; 2(2): 128–149.
45. Mkadmini HK, Hammami M, Rihouey C, et al. Optimization extraction of polysaccharide from Tunisian Zizyphus lotus fruit by response surface methodology: composition and antioxidant activity. *Food Chem* 2016; 212: 476–484.
46. Anguebes F, Abatal M, Bassam A, et al. Esterification optimization of crude African palm olein using response surface methodology and heterogeneous acid catalysis. *Energies* 2018; 11(1): 157.
47. Toft HS, Svenningsen L, Moser W, et al. Assessment of wind turbine structural integrity using response surface methodology. *Eng Struct* 2016; 106: 471–483.
48. Goswami S, Ghosh S and Chakraborty S. Reliability analysis of structures by iterative improved response surface method. *Struct Safety* 2016; 60: 56–66.
49. Ruqayyah TID, Jamal P, Alam MZ, et al. Application of response surface methodology for protein enrichment of cassava peel as animal feed by the white-rot fungus *Panus tigrinus* M609RQY. *Food Hydrocolloids* 2014; 42(2): 298–303.
50. Bezerra MA, Santelli RE, Oliveira EP, et al. Response surface methodology (RSM) as a tool for optimization in analytical chemistry. *Talanta* 2008; 76(5): 965–977.
51. Jiang H, Lai J, Wang C, et al. Research on ranging property of laser radar and its range accuracy. *Chin J Lasers* 2011; 38(5): 0514001.
52. Chen JY. Chinese modern geodetic datum—Chinese Geodetic Coordinate System 2000 (CGCS 2000) and its frame. *Acta Geodaetica Cartographica Sinica* 2008; 37(3): 269–271.
53. Li HP, Bian SF and Li ZM. Chinese Geodetic Coordinate System 2000 and its comparison with WGS84. *Appl Mech Mater* 2014; 580–583: 2793–2796.
54. Kudrys J. Automatic determination of the deflections of the vertical—first scientific results. *Acta Geodynamica Geomaterialia* 2009; 6(3): 233–238.
55. Luo Y, Chen J, Xi W, et al. Analysis of tunnel displacement accuracy with total station. *Measurement* 2016; 83: 29–37.
56. Annan RF, Yao YZ, Ayer J, et al. Accuracy assessment of heights obtained from total station and level instrument using total least squares and ordinary least squares methods. *Geoplanning* 2016; 87(32): 87–92.
57. Xu X, Bureick J, Yang H, et al. TLS-based composite structure deformation analysis validated with laser tracker. *Compos Struct* 2018; 202: 60–65.
58. Liyana-Pathirana C and Shahidi F. Optimization of extraction of phenolic compounds from wheat using response surface methodology. *Food Chem* 2005; 93(1): 53–56.